Available online at www.sciencedirect.com
SCIENCE DIRECT®
Journal of Magnetic Resonance 178 (2006) 33–41
JMR Journal of Magnetic Resonance
www.elsevier.com/locate/jmr

Symmetric spatial encoding in ultrafast 2D NMR spectroscopy

Boaz Shapira, Yoav Shrot, Lucio Frydman *

Department of Chemical Physics, Weizmann Institute of Science, 76100 Rehovot, Israel

Received 21 July 2005; revised 29 August 2005
Available online 4 October 2005

Abstract

Single-scan multidimensional spectroscopy utilizes spatial dimensions for encoding the indirect-domain internal spin interactions. Various strategies have been hitherto demonstrated for fulfilling the encoding needs underlying this methodology; in analogy with their time-domain counterparts all of them have in common the fact that they proceed monotonically—starting at one end of the sample and concluding at the other. The present manuscript discusses another possibility that arises for the case of amplitude-modulated ultrafast *n*D NMR, whereby the spatial encoding progresses from both ends of the sample simultaneously towards the center. Such symmetric encoding is compatible with continuous or discrete excitations as well as with homonuclear or heteronuclear correlations, and exhibits a number of advantages vis-à-vis the unidirectional encodings that have been used so far: it originates echoes that are free from large first-order phase distortions, and yields *n*D peaks possessing a purely-absorptive character. It has the added advantage that for a given indirect-domain spectral resolution it can complete its task in half the time required by a conventional monotonic spatial encoding, leading to potentially important gains in sensitivity. The main features underlying this new spatially symmetric encoding protocol are derived, and its advantages are demonstrated with a series of amplitude-modulated homo- and hetero-nuclear 2D ultrafast NMR examples.

Keywords: Ultrafast 2D NMR; Spatial encoding; Double-frequency-sweep irradiation; TOCSY; HSQC NMR

1. Introduction

Two-dimensional spectroscopy stands at the core of NMR's analytical applications in both chemistry and biochemistry [1–4]. 2D NMR experiments have traditionally relied on time-domain acquisition schemes whereby an initial evolution parameter t_1 encodes the indirect-domain Ω_1 interactions, while a physical time t_2 monitors the direct-domain frequencies Ω_2. Given the Nyquist criteria that govern spectral width and resolution in such Fourier scheme, the collection of numerous t_1-incremented scans becomes an integral part of the data acquisition mode. By contrast to this time-domain encoding an "ultrafast" approach capable of completing the acquisition of complete 2D (and in general of *n*D) NMR spectra within a single scan, has recently been demonstrated [5–7]. Ultrafast 2D NMR owes its single-scan character to a replacement of the serial encoding of the spin interactions occurring in time-domain spectroscopy along t_1, by a parallelized encoding of the interactions along a spatial dimension. A z-dependent chemical shift evolution for instance, can be imparted within a single scan via the combined application of a suitable G_e magnetic field gradient spreading frequencies as $\gamma_e G_e z$, and of frequency selective radiofrequency (RF) pulses exciting spins in a sequential fashion. Fig. 1A exemplifies a simplified scheme that can be used to visualize how such spatially incremented encoding operates, and which we would like to adopt as basis for starting the present discussion. This cartoon assumes the application of a suitably echoed gradient spreading out the spins' resonance frequencies, acting in combination with a monotonic RF sweep scanning this offset range over an evolution period $t_1^{\max}$. As explained elsewhere such scheme can create a spatially dependent magnetization pattern extending throughout the sample's length L, where the internal spin

* Corresponding author. Fax: +972 8 9344123.
E-mail address: lucio.frydman@weizmann.ac.il (L. Frydman).

1090-7807/$ - see front matter © 2005 Elsevier Inc. All rights reserved.
doi:10.1016/j.jmr.2005.08.015

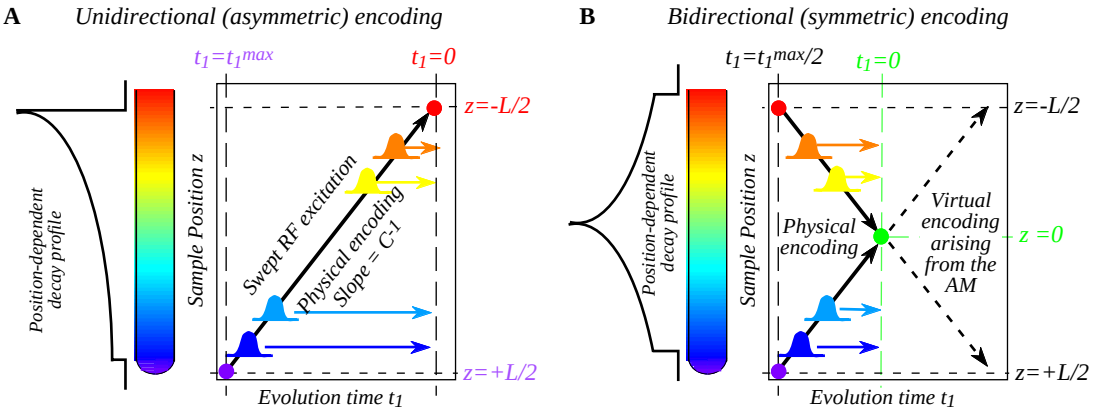

Fig. 1. Comparison between two schemes capable of creating the kind of spatial encoding required for the execution of amplitude-modulated 2D NMR within a single scan. (A) Original protocol whereby the encoding proceeds monotonically from one extreme of the sample to the other, by virtue of a frequency-swept polychromatic RF pulse applied in the presence of a gradient. (B) New scheme discussed in this work whereby the original unidirectional encoding is replaced by a double-frequency sweep proceeding from both ends of the sample towards its center. Notice that due to the amplitude-modulation involved in the experiment, the overall (physical + virtual) encodings imposed by (A) and (B) are identical. Yet the bidirectional scheme yields a symmetric decay envelop whose Fourier conjugate will be free from dispersive contributions, and can be completed in only half the time as its original counterpart.

evolution frequencies Ω_1 have become encoded according to [8]

$$M(z) = A(z)\exp[\mathrm{i}C(\Omega_1 - \Omega_{\mathrm{ref}})(z + L/2)] \times \exp[-C(z + L/2)/T_2^*]. \quad (1)$$

$A(z)$ in this equation represents a density profile for the spins' distribution, which for the conventional high-resolution NMR experiments under consideration we shall assume constant; Ω_{ref} is the rotating-frame offset reference frequency (which for simplicity could be considered zero); and $C = t_1^{\max}/L$ is a controllable parameter describing the efficiency of the spatiotemporal encoding, and thereby the maximum spectral resolution achievable along the indirect-domain. Worth remarking among Eq. (1)'s arguments are the $L/2$ factor arising due to a non-coincidence between the $t_1 = 0$ instant and the $z = 0$ position, as well as the $[\exp -C(z + L/2)/T_2^*]$ decay term multiplying the coherent spin evolution and associated to an effective transverse relaxation.[1]

When inserted within the framework of a 2D NMR acquisition, the indirect-domain evolution embodied by Eq. (1) will be coherently transferred through the pulse sequence's mixing period onto an observable spin, and in general result in a null detectable signal when considering its integration over a $-L/2 \leqslant z \leqslant +L/2$ range of values. The ultrafast NMR detection, however, is implemented while subjecting the sample to an oscillating acquisition field gradient G_a, possessing the same spatial geometry as the initial encoding gradient G_e. The observable NMR signal S becomes then a simultaneous function of the direct-domain time t_2 as well as of a $k = \gamma_a \int_0^t G_a(t')\mathrm{d}t'$ acquisition wavenumber. For the common case of a 2D NMR sequences involving an amplitude modulation of the t_1 evolution, such encoding can be described as

$$S(k, t_2) = \int_{\Omega_2} \left\{ \int_{\Omega_1} I(\Omega_1, \Omega_2) \left[A_o \int_{-L/2}^{+L/2} \cos[C(\Omega_1 - \Omega_{\mathrm{ref}})(z + L/2)] \times \mathrm{e}^{-C(z+L/2)/T_2^*} \mathrm{e}^{\mathrm{i}kz}\,\mathrm{d}z \right] \mathrm{d}\Omega_1 \right\} \mathrm{e}^{\mathrm{i}\Omega_2 t_2} \mathrm{e}^{-t_2/T_2^*}\,\mathrm{d}\Omega_2, \quad (2)$$

where $I(\Omega_1, \Omega_2)$ is the 2D frequency correlation spectrum one is attempting to extract. As can be appreciated from the inner bracketed term in Eq. (2) the k-wavenumber performs a Fourier analysis of the spatially encoded indirect-domain evolution, leading to Ω_1-specific echoes whenever $k = |C(\Omega_1 - \Omega_{\mathrm{ref}})|$. The position of such echoes will thus reveal the nature of the internal spin evolution frequencies, making the k wavenumber equivalent to a ν_1 indirect-domain frequency axis. 2D NMR spectra can then be retrieved within a single scan by oscillating G_a as a function of t_2, and monitoring the modulations that Ω_2 imparts on the direct-domain k-domain echoes via conventional or interlaced Fourier transforms [5,9]. Worth remarking for the sake of completion, is the fact that both discrete as well as continuous versions of the amplitude-modulated spatial encoding protocol just described have been proposed and demonstrated [5,6,8,10]; we shall address relevant aspects of these schemes later in this discussion.

It turns out that regardless of whether discrete or continuous spatial encoding versions are used, a number of artifacts will characterize the point spread functions arising upon subjecting the $S(k/\nu_1, t_2)$ in Eq. (2) to a Fourier transform against t_2 [6,11]. These include a large first-order phase distortion of the peaks stemming from the extra $L/2$ factor pointed out earlier, and mixed-phase components associated to the asymmetric T_2^* relaxation decay affecting both the z- and the t_2-encoded signal intensity profiles. Whereas in principle it is possible to compensate for these two features—the first one by

[1] In actuality an additional exponential decay reflecting potential diffusion effects should be included; yet since its overall influence is akin to that of relaxation its role is not explicitly discussed.

phasing and the second by a procedure that is analogous to a hypercomplex acquisition [12,13]—it would naturally be more convenient if such artifacts were not present at all in the first place. The present contribution describes a way of achieving this aim, based on what we refer to as a symmetric encoding of the spin interactions. When applied to amplitude modulated 2D experiments this procedure has the added advantage of requiring half the time as the hitherto employed spatial encoding schemes, leading to a potentially important increase in sensitivity due to its lessening of relaxation-type decays. The principles underlying this approach are described in the following paragraph, and its performance is subsequently illustrated with a variety of homo- and heteronuclear single-scan 2D acquisitions based on continuous as well as on discrete excitation schemes.

2. Principles and advantages of the spatially symmetric encoding strategy

As happens to be the case in conventional 2D time-domain NMR, the mixed phase components characterizing the ultrafast 2D NMR peaks arising after processing $S(k/v_1, t_2)$ reflect the causality imposed by relaxation during the course of the spin evolution [3,14]. For instance in the spatial encoding scheme depicted in Fig. 1A, where excitation begins at one end of the sample and proceeds monotonically to the opposite extreme, the effects of relaxation distort the ideal, z-independent magnitudes with which spin packets' should contribute to the total signal. Such a break in symmetry about $z = 0$ yields a dispersive contribution upon considering its k/v_1 spectral-domain Fourier conjugate. As discussed elsewhere this problem can be resolved by combining a given data set with its z-decaying mirror-image [11], an encoded/anti-encoded combination where the amplitude-modulated winding described by Eq. (2) is read out via both positive and negative $\pm\gamma_a \int_0^t G_a(t')\mathrm{d}t'$ wavenumber values. A similar kind of symmetry can in principle be created if the monotonic one-way frequency chirp depicted in Fig. 1A, is replaced by a double-frequency sweep taking place in a spatially symmetric way with respect to the $z = 0$ center (Fig. 1B). This will impart an encoding that proceeds simultaneously on two positions within the sample, and which could in principle take place from opposite ends of the sample towards the center, or from the center towards the sample's edges. The first of these choices corresponds to an encoding where the maximum evolution and relaxation decay affect spins positioned at $z = \pm L/2$ whereas spins at $z \approx 0$ have evolved/decayed for the equivalent of $t_1 = 0$.[2] Such an encoding would therefore remove the non-coincidence between the origin of the spatial and temporal frames, an inconsistency that as mentioned earlier is otherwise responsible for large first-order phase distortions resulting in the echo peaks. As this is also an important goal to achieve when considering line shape improvements, we continue the remainder of this presentation by focusing on this kind of symmetric spatial encoding (Fig. 1B) solely.

The double frequency sweep just described can be implemented by replacing the one-way RF modulation underlying Fig. 1A—given in the rotating-frame by $B_1(t) = B_1^0[\cos(\int_0^t O(\tau)\mathrm{d}\tau)\hat{x} + \sin(\int_0^t O(\tau)\mathrm{d}\tau)\hat{y}]$ with $O(\tau)$ an offset being swept at a constant rate R between initial and final values O_i, $O_f = \pm\gamma_e G_e L/2$—by an effective $\pi/2$ pulse whose amplitude is continuously modulated as $B_1(t) = 2B_1^0\cos(\int_0^t O(\tau)\mathrm{d}\tau)\hat{x}$, with $O(\tau) = O_i + R\tau$ now being swept from an initial offset $O_i = |\gamma_e G_e L/2|$ until zero. Just as its one-way counterpart, this symmetric form of spatial encoding will require that the RF be combined with suitably echoed excitation gradients [8]. In principle, the opposite encoding signs imparted by this double-frequency-sweep would seem unsuitable for carrying out an ultrafast experiment, as they imply that a dual winding of magnetizations has now been established on the top and bottom halves of the sample. All resonances along the indirect-domain would thus appear doubled. On the other hand, for the many relevant NMR experiments where an amplitude modulation of the indirect-domain is entailed, the sign difference between these two windings becomes irrelevant. The spatially dependent indirect-domain magnetization pattern imparted on the spins can then be summarized by

$$M(z) = \begin{cases} A_o\cos[+C(\Omega_1 - \Omega_{\mathrm{ref}})z + \Delta] & \\ \quad \times \exp[-Cz/T_2^*], & 0 \leqslant z \leqslant L/2, \\ A_o\cos[-C(\Omega_1 - \Omega_{\mathrm{ref}})z - \Delta] & \\ \quad \times \exp[+Cz/T_2^*], & -L/2 \leqslant z \leqslant 0, \end{cases} \tag{3}$$

where Δ is a constant phase depending on the details of the encoding hardware used, and C takes the same value as in the single-sweep encoding. The resulting magnetization pattern is thus similar to that expected from an amplitude-modulated asymmetric spatial encoding extending over the complete sample; no spectral resolution penalties are incurred by the double-sweep procedure, in spite of having required only half the time ($t_1^{\max}/2$) for achieving its encoding.

The post-mixing echo shapes that will arise upon application of a decoding wavenumber k on the $M(z)$ pattern in Eq. (3), will be given by

$$S(k, t_2) = \int_{\Omega_2}\left\{\int_{\Omega_1} I(\Omega_1, \Omega_2)\left[A_o\int_{-L/2}^{+L/2}\cos[C(\Omega_1 - \Omega_{\mathrm{ref}})z + \Delta]\mathrm{e}^{-C|z|/T_2^*}\mathrm{e}^{\mathrm{i}kz}\,\mathrm{d}z\right]\mathrm{d}\Omega_1\right\}\mathrm{e}^{\mathrm{i}\Omega_2 t_2}\,\mathrm{e}^{-t_2/T_2^*}\,\mathrm{d}\Omega_2. \tag{4}$$

This expression is analogous to Eq. (2), albeit with a couple of important differences. First, it follows that thanks to the spatial symmetry displayed by the relaxation decay

[2] In actuality, the $t_1 = 0$ time will be associated to a shift-dependent position $z_o = \frac{(\Omega_1 - \Omega_{\mathrm{ref}})}{\gamma_e G_e}$, yet for all practical purposes $|z_o|$ is small enough to warrant its replacement by zero.

$\exp(-C|z|/T_2)$ about $z = 0$, the Fourier transformation within brackets will now afford k-domain line shapes that are free from dispersive components along the v_1 indirect domain. This implies that purely absorptive 2D point spread functions will result within a single scan, regardless of which $\pm G_a$ sign is employed in the decoding. A second feature is the absence of $L/2$ factors in the spatial exponents, a consequence of the coincidence imparted between the $z = 0$ coordinate and the $t_1 = 0$ evolution time that frees the indirect-domain line shapes from the large first-order phase distortions that previously affected them.

To further appreciate the overall consequences of the symmetric encoding we compare in Fig. 2 a series of experimental results obtained on a single-site ^{15}N-labeled urea sample, upon using single- and double-frequency sweeps to impose the desired spatial encoding. Shown in Fig. 2A is the indirect-domain spectrum obtained from a single scan upon implementing a ^{1}H–^{15}N HSQC experiment using an asymmetric encoding of the kind introduced in Fig. 1A, where the extent of t_1 evolution maximum at one end of the sample and minimum at the other. As expected the $S(k/v_1, t_2 = 0)$ echo that arises displays both absorptive and dispersive components, severely mixed along the real and imaginary digitizer channels by a first-order phase distortion. Also illustrative is the image arising upon Fourier transforming this k-domain echo peak, whose magnitude provides a spatial profile of the excited sample. The decay observed in such profile (Fig. 2A, bottom) evidences the progressive decoherence occurring over the course of the spatial encoding. Figs. 2B and C compare similar experiments, involving the same encoding gradient and C spatiotemporal factors, but implemented separately over only the top- or bottom-halves of the sample. Despite involving opposite winding senses the $S(k/v_1, t_2 = 0)$ HSQC peaks in these amplitude-modulated experiments appear at identical positions, coinciding with that of their full-sample counterpart. Their line shapes, however, differ from the latter by half-height widths that are now larger due to the smaller extent allowed for their t_1^{max} encoding (only half samples were swept yet at the same absolute rate $|R|$), and by a disappearance of the large first-order phase distortion previously affecting the echo (as for both half-sweeps spins at $z = 0$ have now evolved for $t_1 = 0$ times). Top- and bottom-half echoes also differ in the opposite phasing of their imaginary components, due to the spatial-reversal characterizing the decoherence that has acted on opposite halves of the sample. This in turn helps to visualize why the overall imaginary component will cancel out upon implementing the double-frequency sweep described in the preceding paragraph, as illustrated by the experimental indirect-domain HSQC profile shown in Fig. 2D. In addition to a line shape improvement, this simple example shows what is arguably the main advantage of this new symmetric scheme for the spatial encoding: thanks to the fact that it proceeds simultaneously from both ends of the sample it can achieve the full extent of the spins' evolution encoding in only half the time as its one-way counterpart. This results in z signal profiles that are more weakly affected by decay than those arising from the unidirectional encoding protocol, and consequently in considerably stronger k/v_1 frequency-domain echo peaks. It follows that relying on this new symmetric scheme for carrying out the ultrafast 2D NMR encoding will result in improved purely absorptive point-spread functions as well as in higher sensitivities—without any compromise in the spectral resolution. To the best of our knowledge this is a kind of benefit that has no direct analog in conventional time-domain 2D NMR, being a direct consequence of the parallelization opportunities opened up by the spatial encoding.

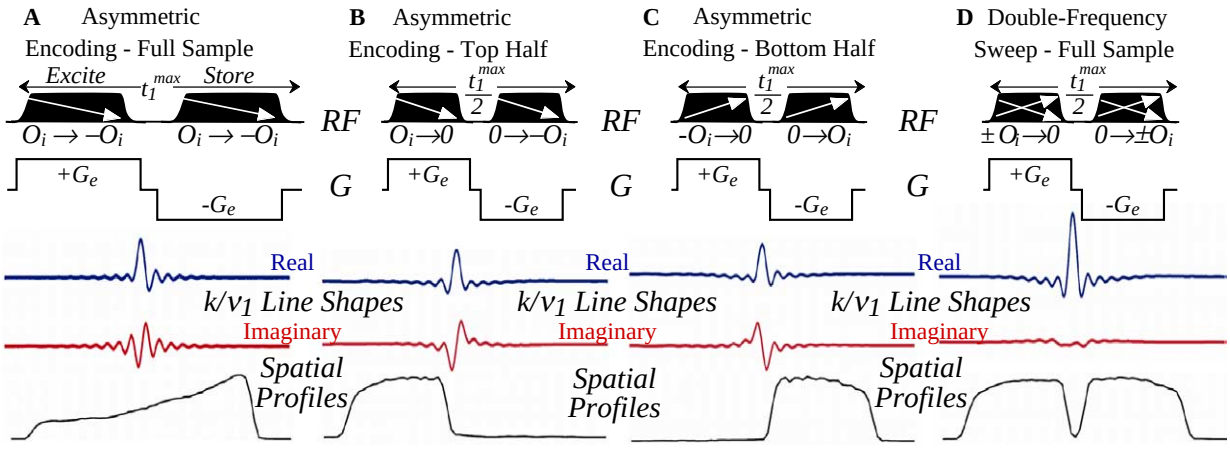

Fig. 2. Outcomes observed upon applying different kinds of asymmetric and symmetric-frequency sweeps on the single ^{1}H-decoupled ^{15}N site of urea. In all cases the starting point of the experiments were single-scan amplitude-modulated 2D HSQC NMR sequences of the type introduced in [8] acquired with the following parameters: $G_e = 35$ G/cm, $|O_i| = 14$ kHz, $t_1^{max} = 100$ ms. Shown underneath each pulse sequence are the line shapes obtained upon decoding the t_1 evolution by applying a 5 G/cm gradient during 1.2 ms—equivalent to an indirect-domain spectral width $SW_1 = 110$ Hz— as well as magnitude representations of the Fourier transform of these k/v_1 echo shapes, corresponding to the decoherence-weighted spatial profiles.

3. Results and discussion

The generality of the symmetric encoding scheme just presented is further investigated in this section with ultrafast 2D NMR analyses based on a continuous encoding of the spin interactions (akin to those in Fig. 2) as well as with applications based on discrete trains of frequency-shifted encoding pulses. These experiments were performed on a Varian iNova 500 MHz NMR spectrometer equipped with an inverse triple-resonance probehead. The various RF and gradient manipulations were implemented via phase- and amplitude-modulating tables generated by the Pbox library of subroutines. All data processing as well as ancillary spin simulations were carried out with custom-written Matlab software packages.

3.1. Symmetric spatial encoding using a continuous RF irradiation

Expanding on the indirect-domain considerations introduced in Fig. 2, we delve here into the character of ultrafast 2D NMR experiments relying on symmetric double-frequency sweeps for carrying out the spins' amplitude-modulation. On applying such form of spatial encoding (Fig. 2D) it follows that spins in the upper portion of the sample become excited by the $+O_i \rightarrow 0$ portion of the RF sweep and subsequently stored by the $0 \rightarrow -O_i$ one, while spins in the lower half undergo a similar process under the action of the $-O_i \rightarrow 0$ and $0 \rightarrow +O_i$ chirps. Under such ideal conditions the arguments put forward in [8] can be followed to calculate the Ω_1 magnetization pattern; aside from an arbitrary phase factor this analysis leads to the results summarized in Eq. (3), with $C = 2\gamma_e G_e/R$ and $\Delta = O_i^2/2R$. The spatio-temporal encoding ratio thus ends up being as efficient as in the case of a conventional sweep while requiring half the overall $t_1^{\max}$, bringing about the benefits that were alluded to earlier.

As for the actual experimental implementation of the double-frequency sweep it was observed that, in order to obtain optimal results, a fine tuning of the purely *cos*-type modulation predicted by theory was required. Indeed maximizing the benefits of the symmetric spatial encoding requires balancing the fates imposed by gradients and pulses on spins positioned on the top and bottom halves of the sample; this in turn requires a certain flexibility to deal with non-idealities such as imbalances that inevitably arise between $+G_e$ and $-G_e$ gradients, gradient switching delays, and other symmetry-breaking phenomena. For instance the first of these non-idealities will shift slightly the coincidence between sub-spectra arising from top and bottom halves of the sample thus compromising the full sensitivity; the latter will prevent a complete cancellation of the dispersive echo components between these two halves, leading to mixed phase line shapes. For the sake of simplicity we chose to compensate all these potential non-idealities at the RF rather than at a gradient or timing levels. Two extra parameters were thus added upon implementing the sweeps: one involved a small frequency offset addition between the RF chirps applied on top and bottom halves of the sample, the other an overall offset that re-defined the spatial "zero" imparted by the double-frequency sweeps. These offsets were in the order of 10–100 Hz (as opposed to the tens of kHz actually involved in the overall frequency sweeps) and, in spite of posing a certain complication, they had the benefit that once properly determined they would remain unchanged regardless of changes in sample or other external modifications.

An experimental demonstration of the overall potential of the double-frequency sweep is illustrated in Fig. 3, which compares different aspects of single-scan 2D TOCSY ^{1}H NMR spectra recorded on a model *n*-butylchloride/$CDCl_3$ sample upon implementing a conventional asymmetric encoding *vs* the new symmetric one. The indirect-domain k/v_1 spectra observable at $t_2 = 0$ (Fig. 3, bottom) evidence, as was illustrated in urea's HSQC acquisition, the new mode's ability to get rid of dispersive components and first-order phase distortions. Moreover, not only are the indirect-domain point-spread functions inherently narrower but also their absolute intensities become substantially higher thanks to the lessened relaxation losses (Fig. 3, bottom).

These combined line shape advantages can be particularly valuable when considering ultrafast *n*D NMR acquisitions on sensitivity-limited samples. To illustrate this Fig. 4 presents another ultrafast 2D example, this time involving a ^{1}H–^{15}N HSQC NMR acquisition on the uniformly ^{13}C/^{15}N enriched labeled tripeptide Leu-Ala-Phe. This sample was dissolved at a 5 mM concentration in a 90/10% H_2O/D_2O buffer, and two scans incorporating Watergate [15] and phase-cycling of the initial heteronuclear pulse (both for the sake of a better water suppression) were collected using asymmetric and symmetric chirped spatial encoding sequences. Representative 2D spectra and 1D cross-sections illustrated in Fig. 4, clearly demonstrate that the two amide cross-peaks arising from the peptide can be discerned with a higher sensitivity and superior overall line shapes when using the double frequency sweep.

3.2. Symmetric spatial encoding involving discrete RF pulses

The symmetric sweep principle can be extended to applications where the spatial encoding is imposed by a discrete train of RF excitation pulses. As discussed elsewhere [5,6] such scheme provides a phase encoding of the spin evolution owing to the application of a train of N_1 pulses of equal duration T_p shifted by constant frequency increments $\Delta O = \gamma_e G_e L/(N_1 - 1)$, in combination with a series of $\pm G_e$ oscillating gradients. The various point-spread-function complications alluded to earlier for the asymmetric continuous encoding will also affect peaks when using this discrete encoding mode [11]; moreover, two additional features absent when dealing with the continuous encoding arise when using this discrete form. These include the

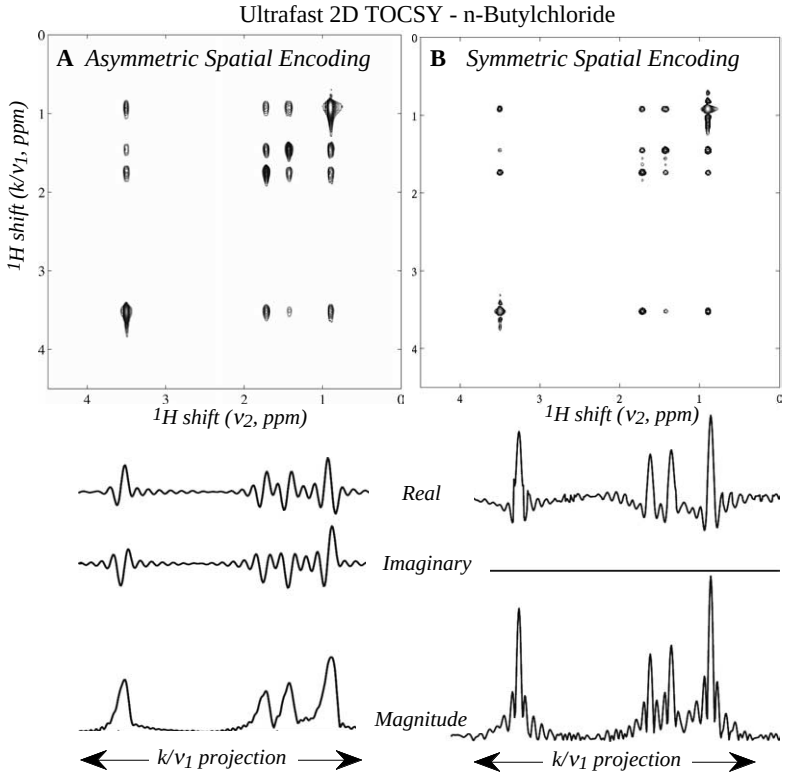

Fig. 3. Comparison between single-scan 2D TOCSY ^{1}H NMR results recorded on *n*-butylchloride/CDCl3 using (A) a conventional one-way spatial encoding of the interactions (as in Fig. 2A). (B) A symmetric spatial encoding of the interactions proceeding simultaneously from both ends of the sample towards the center (as in Fig. 2D). Shown underneath the 2D (magnitude) plots are k/ν_1-traces of the indirect-domain at $t_2 = 0$. Notice the absence of dispersive components and of phase distortions upon using the symmetric encoding scheme, as well the higher intensities afforded by this scheme (all spectra are displayed in an absolute vertical scale). The strong wiggles arising upon using the symmetric encoding result from truncation effects associated to the relatively short indirect-domain evolution times employed (20 ms, leading to an effective $t_1^{max} = 40$ ms). Other acquisition parameters included $G_e = 10$ G/cm, $O_i = \pm 39.5$ kHz, $t_1^{max} = 40$ ms, a decoding gradient $G_a = 40$ G/cm, and 128 t_2 points acquired with a dwell time $\Delta t_2 = 660$ μs.

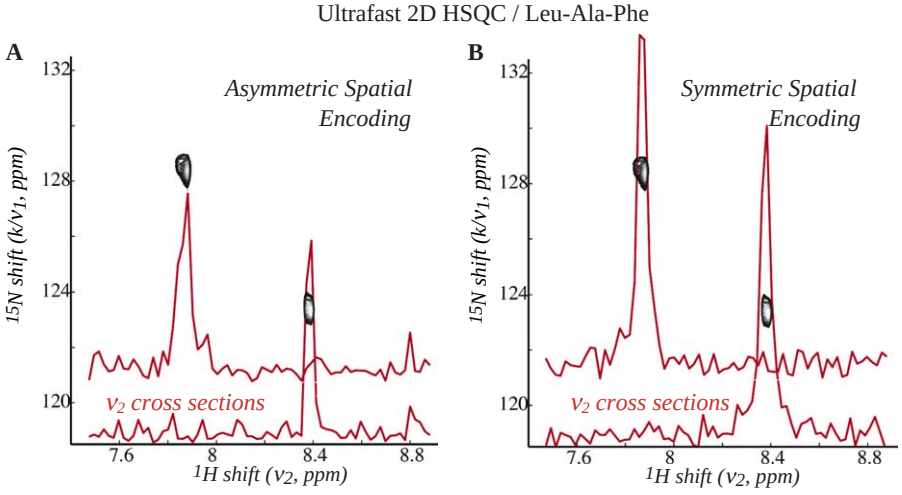

Fig. 4. Summary of ultrafast 2D heteronuclear NMR results obtained on a 5 mM LAF peptide sample when applying a conventional (A) vis-à-vis a symmetric (B) encoding of the spin interactions. Shown for comparison are cross-sections (fixed in their absolute intensities) extracted parallel to ν_2 at the coordinates of the ^{15}N NMR peaks, showing the improvement in sensitivity afforded by the new scheme. The basic pulse sequences used in these tests were continuous HSQC versions of the asymmetric and symmetric sweeps illustrated in Fig. 1, involving the following parameters: $G_e = 40$ G/cm, $O_i = \pm 16$ kHz, $t_1^{max} = 50$ ms, $G_a = 5.4$ G/cm, 70 t_2 points sampled with an effective dwell $\Delta t_2 = 1.44$ ms.

appearance of folded "ghost" peaks arising at $(2T_p)^{-1}$ frequency increments along the ν_1–domain, as well as a *k*-dependent enveloping effect related to the gradient-induced dephasing/rephasing of spin-packets within each discretely excited element. Both of these phenomena have been quantified elsewhere [6,7,16], and end up playing

important roles in the implementation of spatially symmetric encoding schemes in combination with discrete-excitation modes.

To visualize why these effects matter consider the ideal phase-modulated magnetization pattern that any of the B_1 excitation pulses will impose on a z_j-centered discrete slice

$$M(z_j) = A_o\left|\int_{\text{slice}} \mathrm{d}(\delta z)\mathrm{e}^{-\mathrm{i}\gamma_e G_e T_p(\delta z)/2}\cdot B_1^{\mathrm{FT}}(\delta z)\right| \times \exp\{\mathrm{i}[C(\Omega_1-\Omega_{\mathrm{ref}})(z_j+L/2)+\theta]\} \times \exp[-C(z_j+L/2)/T_2^*]. \quad (5)$$

Here the first term within brackets, which was absent in Eq. (1), describes intra-slice dephasing effects depending on the Fourier transform profile of the RF pulse shape (B_1^{FT}). Upon considering the action of the k-wavenumber during the post-mixing acquisition it follows that two concurrent echoing processes will need to take place for observing a signal: one *among* the N_1 excited sub-ensembles and characterizing the indirect-domain frequencies according to echo positions $k=-C(\Omega_1-\Omega_{\mathrm{ref}})$; another *within* each excited slice and endowing the overall indirect-domain spectral intensities with an enveloping profile reflecting the RF pulse shape used in the excitations. When dealing with a conventional spatially asymmetric spin excitation this simultaneity requirement poses no special demands, as the reference offset Ω_{ref} can always be chosen so that both echoing conditions are fulfilled for any given sign of G_a [5,6]. Different, however, would be the situation when carrying out opposite spatial encodings like the ones depicted in Figs. 5A and B, involving the application of $\pi/2$ pulses at frequencies that converge from $+O_i$ and $-O_i$ towards zero while in the presence of a gradient G_e. In such pulse sequences—which are the discrete analogues of the schemes presented in Figs. 2B and C—the inter-slice encoding imparted by the Ω_1 shift will be opposite for spins positioned in the top and bottom halves of the sample (due to the opposing signs of the C factors associated to positive and negative frequency offset increments); yet the intra-slice dephasings will be identical for spins in both halves since in either case they originate under the action of the same gradient G_e. This last consideration implies that only a single sign of k will succeed in unraveling the full phase-modulation encoded during the excitation: the sign that unravels both inter- and intra-slice dephasings. If such k sign satisfies the $k=-C(\Omega_1-\Omega_{\mathrm{ref}})$ condition then genuine indirect-domain peaks will be observed at their correct position, as illustrated by the spectral results appearing on the center column of Fig. 5A. Yet even if this does not happen to be the case and the genuine Ω_1 shift corresponds with the opposite sign of k chosen—which is the case depicted in Fig. 5B, center—echo peaks will *still* be observed owing to the "ghosting" effect mentioned earlier in connection to the discrete excitation. An indirect-domain spectrum with echoes at $k=-C[(2T_p)^{-1}-\Omega_1+\Omega_{\mathrm{ref}}]$ will then arise; notice that because of the reversal in the sign of their apparent k/ν_1 frequency incrementation, such peaks will not appear at the same ν_1-values as in their Fig. 5A counterparts. When considering all these arguments, it becomes clear that the application of double frequency sweeps for the discrete encoding case will not be as straightforward as in the previously discussed continuous scenario. Indeed as a result of applying an encoding that progresses simultaneously from both ends of the sample towards its center a superposition will result, leading to a doubling of all the observable peaks (Fig. 5C, center). Furthermore, no improvement will arise form a mixing process that imposes an amplitude modulation of the spatially encoded interactions, since as illustrated by the experimental traces on the right-hand column of Fig. 5 all that this will cause is

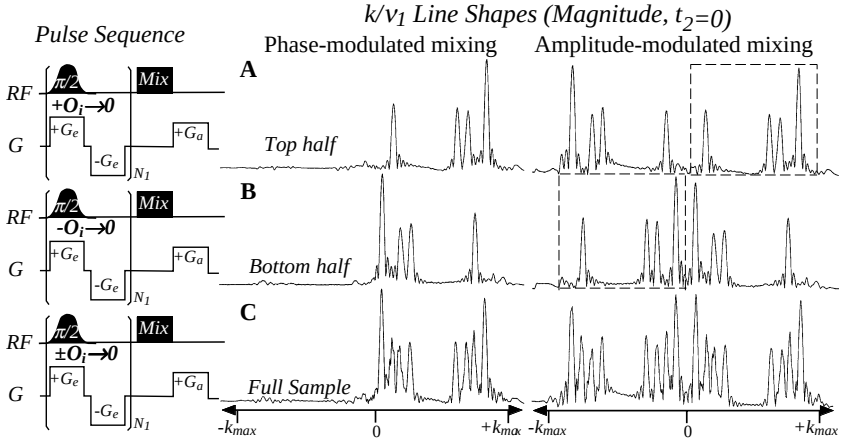

Fig. 5. Complications involved in extending the symmetric encoding principle to a discrete excitation scenario, illustrated with experimental ^{1}H k/ν_1 traces collected on an n-butylchloride/$CDCl_3$ sample. The appearance and positions of peaks are dictated in these instances by ghosting and enveloping phenomena that break the spatial mirror-imaging previously characterizing the encoding on top- and bottom-halves of the sample (e.g., Figs. 2B and C). The key to acquiring coherent spectra from a discrete double-frequency sweep resides in superimposing top- and bottom-half subspectra only after shifting their relative k-positions by the equivalent of the full indirect domain width $k_{\max}$, leading to a superposition of the two regions marked by the dashed boxes. How to implement this, together with experimental parameters related to this figure, is detailed in Fig. 6.

a mirror imaging of the phase-encoded data about the $k = 0$ coordinate. This difference with respect to the continuous encoding behavior (Fig. 2D) is once again a consequence of the combined inter- and intra-slice dephasing effects, which prevent peaks naturally appearing at negative k values from generating echoes at positive k's unless accompanied by a suitable change in their envelop characteristics.

Still, the fact that an amplitude modulation of the spatial encoding creates a mirror-imaging of both the top- and bottom-half spectra, opens up a number of options for reaping the potential benefits arising from symmetric spatial encoding. One possible way to amend this protocol so as to enable it to deal with discrete excitation cases is illustrated by the pulse sequence in Fig. 6. The essence of this sequence, as well as of other conceivable analogues, is to further distinguish among the sub-spectra arising from the top and bottom halves of the sample by imposing on them—in addition to opposed winding directions—an effective k/v_1 shift by a complete width SW_1 on only half of the spins contributing to the total spectrum. Such spatially selective manipulation can be imposed, for example, via the insertion at the conclusion of the indirect-domain evolution of a short gradient in combination with frequency-selective RF pulses, which store at different times the encoding imposed on the top-half and on the bottom-half spin coherences. This can displace the relative k values characterizing the indirect-domain spectra arising from top- and bottom-half spins, leading to a superposition between the boxed traces illustrated in Figs. 5A and B. Following the imposition of an homogeneous mixing process it becomes clear that either positive or negative $\pm G_a$ gradients can then successfully place the indirect-domain spectra arising from top- and bottom-halves back into register, both in terms of their k-domain positions as well as of their spectral enveloping functions. Ultrafast 2D NMR spectra generated under these conditions will thus enjoy from the various benefits inherent to the symmetric spatial encoding—including purely absorptive line shapes, small phase distortions, and an overall enhanced sensitivity—while bypassing the various obstacles depicted in Fig. 5. These various features are experimentally illustrated in the center and lower spectra of Fig. 6, once again using a TOCSY acquisition on an n-butylchloride/$CDCl_3$ model as an example.

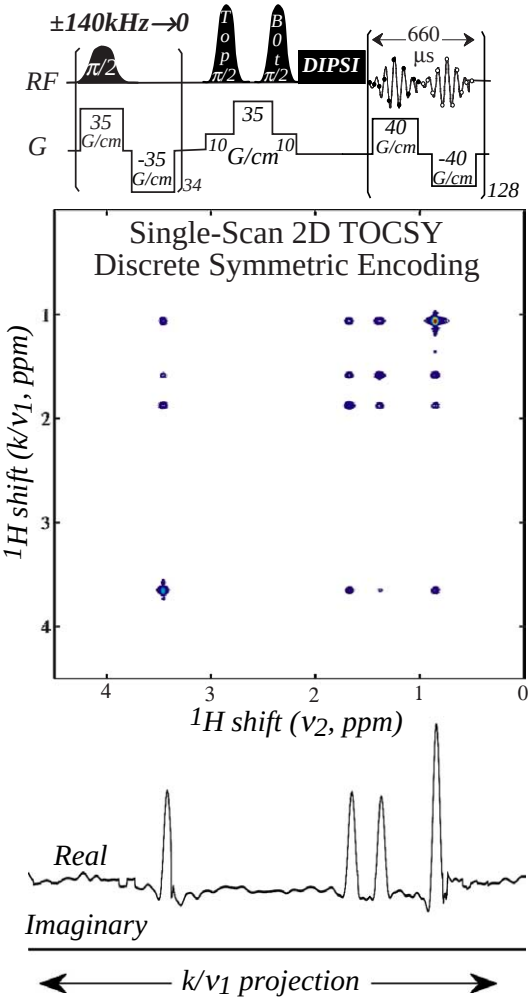

Fig. 6. Implementation of a symmetric encoding using a discrete excitation protocol in single-scan amplitude-modulated 2D NMR. Main differences between the illustrated pulse sequence and the ones involved in a conventional experiment [5,6] include (i) the simultaneous, symmetric excitation of spins residing in both halves of the sample; and (ii) the separate storage of the spins in both halves of the sample, following their initial encoding. The experimental traces illustrate results obtained using the indicated pulse sequence details and a train of 250 µs long selective encoding pulses, 26 µs long spatially selective storage pulses sandwiching a 250 µs long "centering" gradient pulse, and a 60 ms long transverse isotropic mixing. Notice the absence of dispersive components and of first-order phase distortions in the resulting indirect-domain projection (bottom).

4. Conclusions

The double-frequency sweep approach described in this study endows ultrafast 2D NMR experiments with two main advantages over the single-sweep encodings that have hitherto been employed: improved spectral line shapes both in terms of their phasing as well as of their purely absorptive characteristics, as well as sensitivity gains resulting from a more efficient use of the indirect-domain evolution time which brings about an attenuated relaxation. It is interesting to point out that these two main benefits brought about by symmetrization—in both line shape and encoding efficiency—endow incremented-time experiments based on π/2 pulses with advantages that were already built-in when carrying out the spatial encoding by means of constant-time π frequency sweeps [10]. As for the remaining disparities that are known to characterize incremented *vs* constant-time encoding modes, including differences in the effects imposed by homonuclear J couplings and the impact of relaxation on the overall sensitivity, these of course remain unchanged.

Also interesting to point out is the fact that although the present study focused on the application of symmetric encoding to amplitude-modulated ultrafast pulse sequences, its incorporation into suitably modified versions of phase-

modulated schemes can also be conceived. We believe that in combination with other ongoing developments including improvements in the data processing and avenues incorporating sensitivity enhanced schemes, all these proposals could play important roles in facilitating the use of ultrafast NMR. Indeed this progress should assist in making ultrafast 2D NMR a more routine analytical approach for dilute solutions, as well as in extending 3D/4D ultrafast acquisitions beyond the investigation of simple compounds.

Acknowledgments

We are grateful to Dr. Eriks Kupce (Varian) for assistance in setting up the double frequency sweeps, and to Dr. Veronica Frydman (WIS) for the synthesis of the labeled peptide. This work was supported by the Israel Science Foundation (Grant 296/01), the U.S. National Institute of Health (GM-72565), and the German-Israel Fund for Research (GIF 56/2003).

References

[1] J. Jeener, Lecture Presented at Ampere International Summer School II, Basko Polje, Yugoslavia, September 1971.
[2] W.P. Aue, E. Bartholdi, R.R. Ernst, Two dimensional spectroscopy. Application to nuclear magnetic resonance, J. Chem. Phys. 64 (1976) 2229–2246.
[3] R.R. Ernst, G. Bodenhausen, A. Wokaun, Principles of Nuclear Magnetic Resonance in One and Two Dimensions, Clarendon, Oxford, 1987.
[4] J. Cavanagh, W.J. Fairbrother, A.G. Palmer III, N.J. Skelton, Protein NMR Spectroscopy: Principles and Practice, Academic Press, San Diego, 1996.
[5] L. Frydman, T. Scherf, A. Lupulescu, The acquisition of multidimensional NMR spectra within a single scan, Proc. Natl. Acad. Sci. USA 99 (2002) 15858–15862.
[6] L. Frydman, A. Lupulescu, T. Scherf, Principles and features of single-scan two-dimensional NMR spectroscopy, J. Am. Chem. Soc. 125 (2003) 9204–9217.
[7] Y. Shrot, L. Frydman, Single-scan NMR spectroscopy at arbitrary dimensions, J. Am. Chem. Soc. 125 (2003) 11385–11396.
[8] Y. Shrot, B. Shapira, L. Frydman, Ultrafast 2D NMR spectroscopy using a continuous spatial encoding of the spin interactions, J. Magn. Reson. 171 (2004) 162–169.
[9] M. Mishkovsky, L. Frydman, Interlaced Fourier transformation of ultrafast 2D NMR data, J. Magn. Reson. 173 (2005) 344–350.
[10] P. Pelupessy, Adiabatic single-scan 2D NMR spectroscopy, J. Am. Chem. Soc. 125 (2003) 12345–12350.
[11] B. Shapira, A. Lupulescu, Y. Shrot, L. Frydman, Line shape considerations in ultrafast 2D NMR, J. Magn. Reson. 166 (2004) 152–164.
[12] D.J. States, R.A. Haberkorn, D.J. Ruben, A two dimensional nuclear Overhauser experiment with pure absorption phase in four quadrants'', J. Magn. Reson. 48 (1982) 286–292.
[13] D. Marion, K. Wütrich, Application of phase sensitive 2D COSY for measurements of ^{1}H–^{1}H spin–spin coupling constants in proteins, Biochem. Biophys. Res. Commun. 113 (1983) 967–974.
[14] P. Bachmann, W.P. Aue, L. Mueller, R.R. Ernst, Phase separation in two-dimensional spectroscopy, J. Magn. Reson. 28 (1977) 29–39.
[15] M. Piotto, V. Saudek, V. Sklenar, Gradient-tailored excitation for single-quantum NMR spectroscopy of aqueous solutions, J. Biomol. NMR 2 (1992) 661–665.
[16] Y. Shrot, L. Frydman, Ghost-peak suppression in ultrafast two-dimensional NMR spectroscopy, J. Magn. Reson. 164 (2003) 351–356.